

# Non-Fermi liquid behavior in transport across carbon nanotube quantum dots

Leonhard Mayrhofer and Milena Grifoni

*Theoretische Physik, Universität Regensburg, 93040 Germany*

(Dated: June 28, 2018)

A low energy-theory for non-linear transport in finite-size single-wall carbon nanotubes, based on a microscopic model for the interacting  $p_z$  electrons and successive bosonization, is presented. Due to the multiple degeneracy of the energy spectrum diagonal as well as off-diagonal (coherences) elements of the reduced density matrix contribute to the nonlinear transport. A four-electron periodicity with a characteristic ratio between adjacent peaks, as well as nonlinear transport features, in quantitative agreement with recent experiments, are predicted.

PACS numbers: PACS numbers: 73.63.Fg, 71.10.Pm, 73.23.Hk

Since their recent discovery single-wall carbon nanotubes (SWNTs), cf. e.g. [1], have attracted a lot of experimental and theoretical attention. In particular, as suggested in the seminal works [2, 3], due to the peculiar one-dimensional character of their electronic bands, metallic SWNTs are expected to exhibit Luttinger liquid behavior at low energies, reflected in power-law dependence of various quantities and spin-charge separation. Later experimental observations have provided a confirmation of the theory [4, 5]. As typical of interacting electron systems in reduced dimension, SWNTs weakly coupled to leads exhibit Coulomb blockade at low temperatures [6] with characteristic even-odd [7] or four-fold periodicity [8, 9, 10]. In [9] not only the ground state, but also several excited states could be seen in stability diagrams of closed SWNT quantum dots. Such two-fold and four-fold character can be qualitatively understood from symmetry arguments related to the two-fold band degeneracy of SWNTs and the inclusion of the spin degree of freedom. So far, a quantitative description has relied on density functional theory calculations [11] or on a mean field description of the Coulomb blockade [12]. In particular, the position of the spectral lines in the stability diagram measured in [9] was found to be in quantitative agreement with the predictions in [12]. However, a mean field description may be *not* justified for one-dimensional systems. For example, to describe the spectral lines of the sample with four-fold periodicity (sample C) in [9], a quite peculiar choice of the mean field parameters was made, and a quantum dot length three times shorter than the measured SWNT length was assumed. Moreover, to date no quantitative calculation of the nonlinear current across a SWNT dot has been provided.

In this Letter we investigate spectral as well as dynamical properties of electrons in metallic SWNT quantum dots at low energies. We start from a microscopic description of metallic SWNTs and include Coulomb interaction effects, *beyond* mean-field, by using bosonization techniques [2, 3], yielding the spectrum and eigenfunctions of the isolated finite length SWNT. Due to the many-fold degeneracies of the spectrum, the current-voltage characteristics is obtained by solving equations of motion for

the reduced density matrix (RDM) including off-diagonal elements. Analytical results for the conductance are provided, which account for the different heights of the conductance peaks in [9]. Moreover, we can quantitatively reproduce all the spectral lines seen in sample C in [9] by solely using the two ground state addition energies provided in that work. The derived level spacing is in agreement with the measured SWNT length.

To start with, we consider the total Hamiltonian

$$H = H_{\odot} + H_s + H_d + H_T + H_{\text{gate}}, \quad (1)$$

where  $H_{\odot}$  is the interacting SWNT Hamiltonian (cf. Eq. (5) below) and  $H_{s/d}$  describe the isolated metallic source and drain contacts as a thermal reservoir of non-interacting quasi-particles. Upon absorbing terms proportional to external source and drain voltages  $V_{s/d}$ , they read ( $l = s, d$ )  $H_l = \sum_{\sigma\bar{q}} \varepsilon_{\bar{q},l} c_{\bar{q}\sigma l}^{\dagger} c_{\bar{q}\sigma l}$ , where  $c_{\bar{q}\sigma l}^{\dagger}$  creates a quasi-particle with spin  $\sigma$  and energy  $\varepsilon_{\bar{q},l} = \varepsilon_{\bar{q}} - eV_{s/d}$  in lead  $s/d$ . The transfer of electrons between the leads and the SWNT is taken into account by

$$H_T = \sum_{l=s,d} \sum_{\sigma} \int d^3r (T_l(\vec{r}) \Psi_{\sigma}^{\dagger}(\vec{r}) \Phi_{\sigma l}(\vec{r}) + \text{h.c.}), \quad (2)$$

where  $\Psi_{\sigma}^{\dagger}$  and  $\Phi_{\sigma l}^{\dagger}(\vec{r}) = \sum_{\bar{q}} \phi_{\bar{q}}^*(\vec{r}) c_{\bar{q}\sigma l}^{\dagger}$  are electron creation operators in the SWNT and in lead  $l$ , respectively, and  $T_l(\vec{r})$  describes the transparency of the tunneling contact  $l$ . Finally,  $H_{\text{gate}} = -\mu_g \mathcal{N}_c$  accounts for a gate voltage capacitively coupled to the SWNT, with  $\mathcal{N}_c$  counting the total electron number in the SWNT.

*SWNT Hamiltonian.* In the following the focus is on armchair SWNTs at low energies. Then, if periodic boundary conditions are applied, only the gapless energy subbands nearby the Fermi points  $F = \pm \vec{K}_0 = \pm K_0 \hat{e}_x$  with  $\hat{e}_x$  along the nanotube axis, are relevant [2, 3]. To each Fermi point two different branches  $r = R/L$  are associated to the Bloch waves  $\varphi_{R/L,F,\kappa}(\vec{r}) = e^{i\kappa x} \varphi_{R/L,F}(\vec{r})$ , where  $\kappa$  measures the distance from the Fermi points  $\pm K_0$  [2] (Fig. 1a left). In this Letter, however, we are interested in finite size effects. Generalizing [13] to the case of SWNTs we introduce standing waves which fulfill

open boundary conditions (Fig. 1a right):

$$\varphi_{\tilde{R}/\tilde{L},\kappa}^{OBC}(\vec{r}) = \frac{1}{\sqrt{2}} \left[ \varphi_{R/L,K_0,\kappa}(\vec{r}) - \varphi_{L/R,-K_0,-\kappa}(\vec{r}) \right], \quad (3)$$

with quantization condition  $\kappa = \pi(m_\kappa + \Delta)/L$ ,  $m_\kappa$  an integer, and  $L$  the SWNT length. The offset parameter  $\Delta$  occurs if  $K_0 \neq \pi n/L$ , and is responsible for the energy mismatch between the  $\tilde{R}$  and  $\tilde{L}$  branches. Including the spin degree of freedom, the electron operator reads

$$\Psi(\vec{r}) = \sum_{\tilde{r}=\tilde{R},\tilde{L}} \sum_{\kappa,\sigma} \varphi_{\tilde{r}\kappa}^{OBC}(\vec{r}) c_{\tilde{r}\sigma\kappa} =: \sum_{\sigma} \Psi_{\sigma}(\vec{r}), \quad (4)$$

with  $c_{\tilde{r}\sigma\kappa}$  the operator which annihilates  $|\varphi_{\tilde{r}\kappa}^{OBC}\rangle|\sigma\rangle$ . The interacting SWNT Hamiltonian then reads

$$H_{\odot} = \hbar v_F \sum_{\tilde{r}\sigma} \text{sgn}(\tilde{r}) \sum_{\kappa} \kappa c_{\tilde{r}\kappa\sigma}^{\dagger} c_{\tilde{r}\kappa\sigma} + \frac{1}{2} \sum_{\sigma\sigma'} \int d^3r \int d^3r' \Psi_{\sigma}^{\dagger}(\vec{r}) \Psi_{\sigma'}^{\dagger}(\vec{r}') V(\vec{r}-\vec{r}') \Psi_{\sigma'}(\vec{r}') \Psi_{\sigma}(\vec{r}), \quad (5)$$

with  $v_F$  the Fermi velocity. We introduce 1D operators

$$\psi_{\tilde{r}F\sigma}(x) = \frac{1}{\sqrt{2L}} \sum_{\kappa} e^{i\text{sgn}(F)\kappa x} c_{\tilde{r}\sigma\kappa},$$

in terms of which the electron operator in (4) becomes

$$\Psi_{\sigma}(\vec{r}) = \sum_{F,\tilde{r}=\pm} \text{sgn}(F) \sqrt{L} \varphi_{\text{sgn}(F)\tilde{r},F}(\vec{r}) \psi_{\tilde{r}F\sigma}(x), \quad (6)$$

where we used the convention that  $R/L = \pm 1$ ,  $\tilde{R}/\tilde{L} = \pm 1$ . Upon inserting (6) into (5), integration over the coordinates perpendicular to the tube axis yields the interacting Hamiltonian expressed in terms of 1D operators and an effective 1D interaction  $V_{eff}(x, x')$ . Using standard bosonization techniques [2, 3]  $H_{\odot}$  can now be diagonalized when keeping only forward scattering processes associated to  $V_{eff}(x, x')$ . It reads

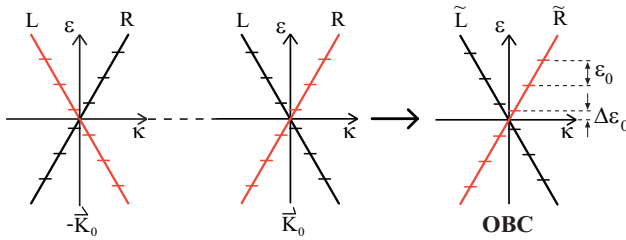


FIG. 1: Energy spectrum of a SWNT with open boundary conditions (right) described in terms of left ( $\tilde{L}$ ) and right ( $\tilde{R}$ ) branches. It is constructed from suitable combinations of travelling waves whose spectrum is shown on the left side.

$$H_{\odot} = \frac{1}{2} E_c \mathcal{N}_c^2 + \varepsilon_0 \sum_{\tilde{r}\sigma} \left( \frac{\mathcal{N}_{\tilde{r}\sigma}^2}{2} + \Delta \text{sgn}(\tilde{r}) \mathcal{N}_{\tilde{r}\sigma} \right) + \sum_{q>0} \sum_{j=c,s} \sum_{\delta=\pm} \varepsilon_{j\delta q} a_{j\delta q}^{\dagger} a_{j\delta q}, \quad (7)$$

where the first line is the fermionic contribution and represents the energy cost, due to Pauli's principle and the Coulomb interaction, of adding new electrons to the system. Specifically,  $\mathcal{N}_{\tilde{r}\sigma} = \sum_{\kappa} c_{\tilde{r}\sigma\kappa}^{\dagger} c_{\tilde{r}\sigma\kappa}$ , is the operator that counts the number of electrons in the ( $\tilde{r}\sigma$ )-branch,  $\mathcal{N}_c = \sum_{\tilde{r}\sigma} \mathcal{N}_{\tilde{r}\sigma}$  yields the total electron number, and  $\varepsilon_0 = \hbar v_F \frac{\pi}{L}$  is the free-particle level spacing (see Fig. 1). The term  $E_c = W_{00}$  is the SWNT charging energy, where  $W_{qq} = \frac{1}{L^2} \int_0^L dx \int_0^L dx' V_{eff}(x, x') \cos(qx) \cos(qx')$ . The second line of (7) describes bosonic excitations in terms of the bosonic operators  $a_{j\delta q}$ . Four channels are associated to total ( $j\delta = c+, s+$ ) and relative ( $j\delta = c-, s-$ ) (with respect to the occupation of the  $\tilde{R}$  and  $\tilde{L}$  branch) charge and spin excitations. Generalized spin-charge separation occurs, since for three of the channels the energy dispersion is the same as for the noninteracting system,  $\varepsilon_{j\delta q} = \hbar v_F q = \hbar v_F \frac{\pi}{L} n_q =: \varepsilon_0 n_q$ , ( $n_q$  a positive integer), but the ( $c+$ ) channel is affected by the interaction with  $\varepsilon_{c+q} = \varepsilon_0 n_q (1 + 8W_{qq}/\varepsilon_0)^{1/2}$ . The eigenstates are

$$\prod_{q>0,j\delta} (m_{j\delta q}!)^{-1/2} \left( a_{j\delta q}^{\dagger} \right)^{m_{j\delta q}} |\vec{N}, \vec{0}\rangle =: |\vec{N}, \vec{m}\rangle, \quad (8)$$

where  $|\vec{N}, \vec{0}\rangle$  has no bosonic excitations and  $\vec{N}$  defines the number of electrons in each of the branches ( $\tilde{r}\sigma$ ).

*Dynamics.* Our starting point to describe transport in SWNTs is the exact equation of motion

$$i\hbar \frac{\partial \rho^I(t)}{\partial t} = Tr_{leads} [H_T^I(t), W^I(t)], \quad (9)$$

for the reduced density matrix (RDM)  $\rho^I = Tr_{leads} W^I$  of the SWNT. Here  $W^I(t)$  is the density matrix of the whole system consisting of the leads and the quantum dot, and  $Tr_{leads}$  indicates the trace over the lead degrees of freedom. The apex  $I$  denotes the interaction representation with  $H_T$  from (2) as the perturbation. We make the following approximations: i) We assume weak coupling to the leads, and treat  $H_T$  up to second order, i.e., we consider the leads as reservoirs which stay in thermal equilibrium and make the factorization ansatz  $W^I(t) = \rho^I(t) \rho_s \rho_d =: \rho^I(t) \rho_{leads}$  where  $\rho_{s/d} = Z_{s/d}^{-1} e^{-\beta(H_{s/d} - \mu_{s/d} \mathcal{N}_{s/d})}$ , with  $Z_{s/d}$  the partition function and  $\beta$  the inverse temperature. ii) Being interested in long time properties, we can make the so called Markov approximation, where the time evolution of  $\rho^I(t)$  is only local in time. iii) Since we know the eigenstates  $|\vec{N}, \vec{m}\rangle$  of  $H_{\odot}$ , it is convenient to calculate the time evolution of  $\rho^I$  in this basis. We assume that matrix elements between states representing a different number of electrons (charge states) in the SWNT and with different energies vanish. Coherences between degenerate states with the same energy  $E$  are retained! Hence we can divide  $\rho^I(t)$  into block matrices  $\rho_{nm}^{I,E,N}(t)$ , where  $E, N$  are the energy and number of particles in the degenerate eigenstates  $|n\rangle$ ,

$|m\rangle$ . We arrive at equations of the Bloch-Redfield form

$$\begin{aligned} \rho_{nm}^{I,E_N}(t) = & - \sum_{kk'} R_{nm\,kk'}^{E_N} \rho_{kk'}^{I,E_N}(t) \\ & + \sum_{E'} \sum_{M=N\pm 1} \sum_{kk'} R_{nm\,kk'}^{E_N\,E'_M} \rho_{kk'}^{I,E'_M}(t), \end{aligned} \quad (10)$$

where  $k, k'$  run over all degenerate states with fixed particle number. The Redfield tensors are given by ( $l = s, d$ )

$$R_{nm\,kk'}^{E_N} = \sum_l \sum_{E', M, j} \left( \delta_{mk'} \Gamma_{l,njjk}^{(+)\,E_N\,E'_M} + \delta_{nk} \Gamma_{l,k'jjm}^{(-)\,E_N\,E'_M} \right), \quad (11)$$

and  $R_{nm\,kk'}^{E_N\,E'_M} = \sum_{l,\alpha=\pm} \Gamma_{l,k'mnk}^{(\alpha)\,E'_M\,E_N}$ , where the quantities  $\Gamma_{l,njjk}^{(\alpha)\,E_N\,E'_M}$  are transition rates from a state with  $N$  to a state with  $M$  particles. Known the stationary density matrix  $\rho_{st}^I$ , the current (through lead  $l$ ) follows from

$$I = 2\text{Re} \sum_{N,E,E'} \sum_{nkj} \left( \Gamma_{l,njjk}^{(+)\,E_N\,E'_{N+1}} - \Gamma_{l,njjk}^{(+)\,E_N\,E'_{N-1}} \right) \rho_{kn,st}^{I,E_N}. \quad (12)$$

iv) We exploit the localized character of the transparencies  $T_l(\vec{r})$  in Eq. (2), and make use of the slowly varying nature of the operator  $\psi_{\vec{r}F\sigma}(x)$  in Eq. (6). This enables us to evaluate the 1D operator at the SWNT contacts and pull it out from the space integrals which enter the definition of the transition rates. It holds  $\langle r | \psi_{\vec{r}\sigma F}(x=0) | s \rangle := (\psi_{\vec{r}\sigma})_{rs}^{E_N\,E'_{N+1}}$ ;  $\langle r | \psi_{\vec{r}\sigma F}(x=L) | s \rangle = e^{-i\pi \text{sgn}(F) \{ \mathcal{N}_{\vec{r}\sigma \text{sgn}(\vec{r}) + \Delta} \}} (\psi_{\vec{r}\sigma})_{rs}^{E_N\,E'_{N+1}}$  for the matrix elements between the states  $|r\rangle, |s\rangle$  with energy  $E, E'$  and particle number  $N, N+1$ , respectively. We thus can introduce

$$\begin{aligned} \Phi_{l\vec{r}\vec{r}'}(\varepsilon) = & \int d^3r \int d^3r' T_l(\vec{r}) T_l(\vec{r}') \sum_{\vec{q}_l} \phi_{l\vec{q}}(\vec{r}) \phi_{l\vec{q}}^*(\vec{r}') \\ & \times \sum_{FF'} \text{sgn}(FF') \varphi_{\text{sgn}(F)\vec{r},F}(\vec{r}) \varphi_{\text{sgn}(F')\vec{r}',F'}(\vec{r}') \eta_l(\Delta), \end{aligned}$$

to describe the influence of the geometry of a tunneling contact at the tube end. The term  $\eta_l(\Delta) = e^{i\pi \text{sgn}(F-F')\Delta(1-\delta_{l,d})}$  accounts for the mismatch  $\Delta$ . Assuming a 3D electron gas in the leads, e.g. of gold, we find that for a realistic range of energies is  $\Phi_{l\vec{r}\vec{r}'}(\varepsilon) = \delta_{\vec{r}\vec{r}'} \Phi_l$ , i.e. the leads are "unpolarized". We thus obtain

$$\begin{aligned} \Gamma_{l,rs's'r'}^{(\pm)\,E_N\,E'_{N+1}} = & \frac{1}{\hbar^2} \sum_{\vec{r}\sigma} \int d\varepsilon \rho_l^\oplus(\varepsilon) \Phi_l(\varepsilon) (\psi_{\vec{r}\sigma})_{rs}^{E_N\,E'_{N+1}} \\ & \times \left( \psi_{\vec{r}\sigma}^\dagger \right)_{s'r'}^{E'_{N+1}\,E_N} \int_0^\infty dt' e^{\pm \frac{i}{\hbar}(\varepsilon - eV_l - (E' - E))t'}, \end{aligned} \quad (13)$$

with  $\rho_l^\oplus(\varepsilon) = \rho_l(\varepsilon)f(\varepsilon)$ , where  $\rho_l(\varepsilon)$  is the density of en-

ergy levels in lead  $l$ , and  $f(\varepsilon)$  the Fermi function. Alike,

$$\begin{aligned} \Gamma_{l,rs's'r'}^{(\pm)\,E_N\,E'_{N-1}} = & \frac{1}{\hbar^2} \sum_{\vec{r}\sigma} \int d\varepsilon \rho_l^\ominus(\varepsilon) \Phi_l(\varepsilon) \left( \psi_{\vec{r}\sigma}^\dagger \right)_{rs}^{E_N\,E'_{N-1}} \\ & \times (\psi_{\vec{r}\sigma})_{s'r'}^{E'_{N-1}\,E_N} \int_0^\infty dt' e^{\mp \frac{i}{\hbar}(\varepsilon - eV_l + (E' - E))t'}, \end{aligned} \quad (14)$$

with  $\rho_l^\ominus(\varepsilon) = \rho_l(\varepsilon)(1 - f(\varepsilon))$ .

*When are coherences needed?* Eqs. (10) with (12) show that coherences (in the energy basis) enter the evaluation of the current. In the low bias and temperature regime  $k_B T, eV := e(V_s - V_d) \ll \varepsilon_0$ , however, where only ground states contribute to the current, because of  $\langle \vec{N}, \vec{0} | \psi_{\vec{r}\sigma}^\dagger \psi_{\vec{r}\sigma} | \vec{N}', \vec{0} \rangle = (1/2L) \delta_{\vec{N}', \vec{N}}$ , only diagonal elements of the RDM contribute. Hence, due to the "unpolarized" character of the leads, the commonly used master equation (CME) with population's dynamics only is valid. At larger biases coherences should be included [14].

In the following we focus on the case  $\Delta \approx 0$ , relevant to explain the experimental results for sample C in [9].

*Low bias regime (CME is valid).* At low bias the current can be obtained by looking to transitions between ground states with  $N$  and  $N+1$  particles and energies  $E_N^0, E_{N+1}^0$ . Then, the matrix element  $(\psi_{\vec{r}\sigma})_{\vec{N}', \vec{N}}$  is non zero only if  $\vec{N}' = \vec{N} - \hat{e}_{r\sigma}$ , with  $\hat{e}_{r\sigma}$  the unit vector, and

$$\sum_{\vec{N}'} \sum_{\vec{r}\sigma} (\psi_{\vec{r}\sigma}^\dagger)_{\vec{N}\vec{N}'} (\psi_{\vec{r}\sigma})_{\vec{N}'\vec{N}} = \frac{1}{2L} C_{N,N'}. \quad (15)$$

Here  $C_{N,N'}$  is the number of ground states with  $N'$  particles whose configurations  $\vec{N}'$  differ from the fermionic configuration of a given ground state with  $N$  electrons only by a unit vector. With  $N = 4m, 4m+1, 4m+2, 4m+3$  one finds  $C_{N,N+1} = 4, 3, 2, 1$  and  $C_{N+1,N} = 1, 2, 3, 4$ , respectively. We also notice that all ground states with  $N$  particles are populated with equal probability, such that we can introduce the occupation probability  $P_N(t) = d_N \rho_{\vec{N}, \vec{N}}(t)$ , where  $d_N$  is the degeneracy of the ground states with particle number  $N$ . It holds  $d_N/d_{N+1} = C_{N+1,N}/C_{N,N+1}$ . The corresponding CME for  $P_N(t)$  can now be easily solved and the current evaluated in analytic form. We find

$$|I_{N,N+1}| = \frac{e\Delta f C_{N,N+1} C_{N+1,N} \gamma_s \gamma_d}{\sum_{l=s,d} \gamma_l [C_{N,N+1} f(\varepsilon_l) + C_{N+1,N} (1 - f(\varepsilon_l))]}, \quad (16)$$

where  $\Delta f = |f(\varepsilon_s) - f(\varepsilon_d)|$ ,  $\varepsilon_l = eV_l - \Delta E$ , and  $\Delta E = E_N^0 - E_{N+1}^0$ . Moreover,  $\gamma_l = (\pi/L\hbar) \Phi_l \rho_l(0)$ . This expression can be further simplified in the regime  $|eV| \ll kT \ll \varepsilon_0$  where the linear conductance  $G_{N,N+1}$  is obtained by linearizing  $\Delta f$  in  $V$ , and by evaluating the remaining quantities in (16) at zero bias. The conductance trace exhibits four-electron periodicity (Fig. 2a), with two equal in height central peaks for the transitions  $N = 4m+1 \rightarrow N+1$ ,  $N = 4m+2 \rightarrow N+1$ , and two

smaller peaks for  $N = 4m \rightarrow N+1$ ,  $N = 4m+3 \rightarrow N+1$  also equal in height. The relative height between central and outer peaks is  $G_{4m+1, 4m+2}^{max}/G_{4m, 4m+1}^{max} = 27/(10 + 4\sqrt{6}) \approx 1.36$ , independent of the ratio  $\gamma_s/\gamma_d$ .

In the bias regime  $\varepsilon_0 \gg |eV_i \pm \Delta E| \gg kT$  is  $\Delta f = 1$ . If e.g.  $eV_s - \Delta E < 0$  and  $eV_d - \Delta E > 0$ , such that tunneling is preferable from source to drain, we find  $I_{N, N+1} = eC_{N, N+1}C_{N+1, N}\gamma_s\gamma_d/(\gamma_s C_{N, N+1} + \gamma_d C_{N+1, N})$ . In this regime, the nonlinear conductance will still exhibit four-electron periodicity, Fig. 2b. For  $\gamma_s = \gamma_d$  one still expects two equal central peaks and two smaller outer peaks with ratio 3/2. If  $\gamma_s \neq \gamma_d$  this latter symmetry is lost. If we invert the sign of the bias voltage, the current is obtained by exchanging  $\gamma_s$  with  $\gamma_d$ .

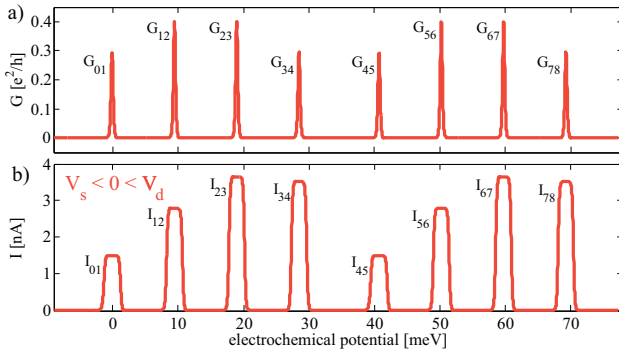


FIG. 2: a) Conductance vs. electrochemical potential in the linear regime  $eV \ll k_B T \ll \varepsilon_0$ . Despite asymmetric contacts, the two central peaks and the two outer peaks have equal height. b) Current in the regime  $\varepsilon_0 \gg |eV_i| \gg kT$ . Asymmetry effects become visible. Four-electron periodicity is still observed. Parameters are  $E_c = 9.5$  meV;  $k_B T = 0.10$  meV,  $\varepsilon_0 = 2.9$  meV,  $\gamma_s = 5\gamma_d = 4.9 \cdot 10^{10} s^{-1}$ .

*High bias regime.* In the bias regime  $eV > \varepsilon_0$  states with bosonic as well as fermionic excitations contribute to transport. An analytical treatment is not possible, except to define the position of the various excitation lines. The resonance condition for tunneling in/out of lead  $l$  is as usually given by  $eV_l + \Delta E^\pm = 0$ , where  $\Delta E^\pm = \pm(E_{N\pm 1} - E_N)$ . Besides the resonance condition, also the overlap integral between initial and final state determines the rates, and hence the "active" resonance lines contributing to the current. Fig 3a shows the current in a bias voltage-electrochemical potential plane for the symmetric case  $\gamma_s = \gamma_d$ . By choosing the addition energies provided in [9]  $\Delta\mu_1 = E_c = 9.5$  meV and  $\Delta\mu_2 = 13.4$  meV, we can reproduce all the excitation lines from sample C in [9]. Moreover, we find a level spacing  $\varepsilon_0 = 2.9$  meV, which well agrees with the estimated length for sample C of 750 nm. We compare with the mean field parameters: to fit the data, an unusually large exchange interaction  $J = 2.9$  meV as well as a band shift  $\varepsilon_0\Delta \approx J$  had to be assumed in [9] (in our theory is  $\varepsilon_0\Delta \approx J \approx 0$ ). This yields a level spacing three times

larger than the one obtained from our treatment and not consistent with the measured SWNT length.

Finally, the effect of the coherences induced by the bosonic excitations is shown in Fig. 3b, where a difference plot for the current with and without coherences is shown. Though the coherences do not qualitatively change the current, they do have a quantitative influence in a region of intermediate bias  $V$ . A further indication for non-Fermi liquid behavior could lie in negative differential (NDC) features originating from spin-charge separation, as predicted for a spinful Luttinger liquid quantum dot [15]. Asymmetric contacts are a necessary requirement. We checked these predictions as possible explanation of the NDC seen in [9]. We confirm that (also for non-relaxed bosons) NDC occurs. However, very large asymmetries must be assumed. Moreover, in contrast to the experiments, all the NDC lines have the same slope.

To conclude, we discussed linear and nonlinear transport in SWNT quantum dots using a bosonization approach. Our results are in quantitative agreement with experimental findings in [9]. Further work to explain the nature of the NDC seen in [9] is needed.

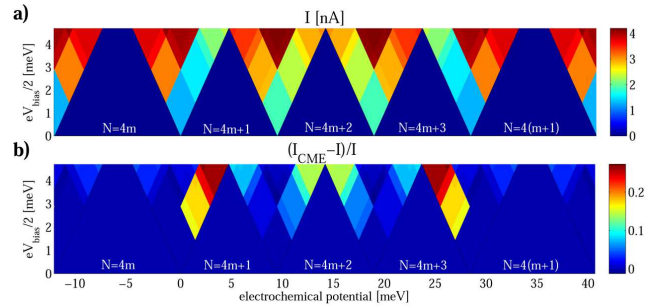


FIG. 3: a) Current in a bias voltage - electrochemical potential plane for the symmetric contacts case. b) Difference plot of the current with and without coherences. Here  $k_B T = 0.01$  meV and  $\varepsilon_0/\varepsilon_{c+q} \approx 0.21$ . Other parameters are as in Fig. 2a.

\*\*\*

Useful discussions with S. Sapmaz and support by the DFG under the program GRK 638 are acknowledged.

- 
- [1] R. Saito, G. Dresselhaus, M. Dresselhaus, *Physical Properties of Carbon nanotubes* (Imperial College Press. London 1998).
  - [2] R. Egger and A. O. Gogolin, Phys. Rev. Lett. **79**, 5082 (1997); Eur. Phys. J. B **3**, 281 (1998).
  - [3] C. Kane, L. Balents and M. P. A. Fisher, Phys. Rev. Lett. **79**, 5086 (1997).
  - [4] M. Bockrath *et al.*, Nature **397**, 598 (1999).
  - [5] H. W. Ch. Postma *et al.*, Science **293**, 76 (2001).
  - [6] S. J. Tans *et al.*, Nature **386**, 474 (1997).
  - [7] D. H. Cobden and J. Nygård, Phys. Rev. Lett. **89**, 046803 (2002).

- [8] W. Liang, M. Bockrath and H. Park, Phys. Rev. Lett. **88**, 126801 (2002).
- [9] S. Sapmaz *et al.*, Phys. Rev. B **71**, 153402 (2005).
- [10] S. Moriyama *et al.*, Phys. Rev. Lett. **94**, 186806 (2005).
- [11] S.-H. Ke, H. U. Baranger and W. Yang, Phys. Rev. Lett. **91**, 116803 (2003).
- [12] Y. Oreg, K. Byczuk and B. I. Halperin, Phys. Rev. Lett. **85**, 365 (2000).
- [13] M. Fabrizio, A. O. Gogolin, Phys. Rev. B **51**, 17827 (1995).
- [14] In the case of noninteracting electrons and unpolarized leads, the CME is always correct if the usual Bloch wave Slater determinants are used as energy eigenstates.
- [15] F. Cavaliere *et al.*, Phys. Rev. Lett. **93**, 036803 (2004).